Science of Sintering, **54** (2022)439-448

https://doi.org/10.2298/SOS2204439I

UDK: 546.74; 692.533.1; 539.375

Wear and Microstructural Properties of Ni-B_4C/CNF Composites

Serkan Islak[1*)], Vahdettin Koç[2], Abdualkarim Musbah M. Gariba[3]

[1]Kastamonu University, Faculty of Engineering and Architecture, Department of Mechanical Engineering, Kastamonu-Turkey

[2]Adıyaman University, Vocational High School of Technical Sciences, Adıyaman-Turkey

[3]Kastamonu University, Institute of Science, Kastamonu-Turkey

Abstract:

The aim of this study is to investigate the microstructure and wear properties of nickel (Ni) matrix boron carbide (B_4C) and carbon nanofiber (CNF)-reinforced composite materials. Microstructure and phase composition of the composites manufactured by powder metallurgy (PM) method were determined by SEM-EDS and XRD analysis. While hardness values of the composites were determined by Vickers hardness measurement method, their wear properties were determined by using pin-on-disc method. SEM images showed that B_4C was homogeneously distributed, but CNF accumulated in some areas, even though it was slight. Addition of B_4C and CNF to the matrix significantly increased it. The increase was quite high in B_4C addition, and hardness was slightly lower in the addition of CNF. According to the results of the wear test carried out under dry conditions, the reinforcement to the Ni matrix reduced the wear rate and friction coefficient.

Keywords*: Nickel; Carbon nanofiber; Boron carbide; Wear; Composites.*

1. Introduction

Ni-based alloys used for high temperature applications have some outstanding properties such as excellent mechanical strength, good thermal stability and chemical inertness [1]. Due to these properties, nickel alloys are used in chemical industry, petroleum industry, glass mold industry, hot work punches, fan blades and sludge disposal elements in cement plants, coal boilers, heat exchangers, turbines, pistons, agricultural machinery, medical applications, spacecraft, and nuclear power systems as well as machines and parts subjected to wear and high temperature corrosion, such as heat treatment equipment [2]. Higher-quality materials are produced by manufacturing ceramic-reinforced composites with nickel matrix. Wu et al., [3] produced the SiC Coated α-Al_2O_3- reinforced Ni Matrix composite and investigated the mechanical behaviours of this composite. The yield strength of heat-treated composite has been reported to be six times that of pure Ni. Islak et al. [4] added TiC at different rates into the Ni-based alloy and produced the NiCrBSi-TiC composite by employing the hot press technique. The authors pointed out that as the TiC rate increased, the friction coefficients decreased and the hardness increased. By adding B of different rates into Ni-TiC composite, Akkaş and Islak [5] investigated the microstructure, wear, and corrosion properties of boron. Hard boride forming in the matrix and the TiC particles added externally have been reported to increase the wear resistance of the composite and decrease its

[*)] **Corresponding author:** serkan@kastamonu.edu.tr

corrosion resistance. Buytoz et al. [6] manufactured NiCrBSi-SiC composite on SAE 1030 steel surface by HVOF method. It is stated that carbide and boride phases have formed in the microstructure, generating significant increases in wear resistance and hardness.

Ni-matrix composites are produced with the addition of nano-dimensional particles, as well as ceramic-based micro-particles. This enables superior properties to be acquired. Jiang et al. [7] produced graphene-nickel composites by using the in-situ method. The graphene has been reported to be homogeneously dispersed in nickel, form an excellent interface with the matrix and have an outstanding load-bearing property. Nguyen et al. [8] added 0.1 wt.% CNT to Ni and produced composites by spark plasma sintering. When compared to unreinforced Ni, composite has been reported to have higher hardness and an acceptable tensile strength, but lower ductility.

Upon the literature review, it has been understood that there is a limited number of carbon nano-fibre-reinforced Ni-matrix composites and Ni-B_4C-CNF composite has been not studied at all. This study investigated the microstructure and wear properties of the Ni-B_4C-CNF composite produced by the powder metallurgy method.

2. Materials and Experimental Procedures

In this study, nickel powder (Purity, 99.95 %; particle size, 325 mesh) as matrix and B_4C (Purity, 99.95 %; particle size, 325 mesh) and CNF (diameter: 100 nm, size: 20-200 μm, purity >98 %) powders as reinforcement were used. Fig. 1 shows SEM images of the powders used. While the morphology of nickel powder is typically spherical, the boron carbide powder has a complex shape and sharp corners, and the carbon nano-fibres, on the other hand, have a fibrous morphology. The powders weighed on the precision scale at the mixture rates given in Table I were mixed in the mechanical alloying device (Retsch PM 100) for 2 h at rotation speed of 350 rpm in the ratio of 10:1. 100Cr6 steel balls with a diameter of 10 mm were utilized for the mixture process. In order to prevent cold welding and combustion, 2 wt.% of zinc stearate was added to the powder mixture. The powder mixtures were then pressed at 500 MPa in the 13-mm diameter moulds. The pressed samples were sintered for one hour at 950^{o}C at heating/cooling rate of 10^{o}C/min in a tube furnace with shielding argon gas atmosphere. As can be seen from Table I, a total of five groups of samples and three samples in each group were produced.

Tab. I Powder mixture rates.

Sample No.	Ni (vol.%)	B_4C (vol.%)	CNF (vol.%)
1	100	0	0
2	90	10	0
3	89	10	1
4	88.5	10	1.5
5	88	10	2

The samples were sanded on 320-2400 mesh sandpaper and polished using a diamond solution for the microstructure analysis. The samples were etched in the solution of 100 ml distilled water + 25 ml hydrochloric acid + 8 g iron (III) chloride. X-ray diffraction (XRD) analysis was done by using Bruker D8 Advance device (Bruker Optik GmbH, Ettlingen, Germany). Scanning electron microscope (SEM) and energy dispersive spectrometer (EDS) analyses were done by using FEI QUANTA 250 FEG device (FEI Inc., OR, USA). In order to understand the sintered densities, the densities of all samples produced were measured with a 10^{-4} precision AND GR-200 brand balance (AND, Japan) according to the Archimedes' principle as specified in the ASTM B 962-17 standard [9]. The experimental densities were divided by the calculated theoretical densities to calculate the relative densities. The samples' hardness was measured with a SHIMADZU HMV-G21 microhardness instrument (HMV-G21ST, SHIMADZU, Japan) under a 1 kg load and for a 16-second wait time according to ASTM E92−17 standard [10]. Pin-on-disc wear test was applied to all samples in accordance with ASTM G99-17 standard [11], using a UTS Tribometer T10 tester (T10, UTS Tribometer, Turkey). Tests were conducted under room conditions at a 10N load and a dislocation distance of 350 m. The data collection rate was selected at 3 Hz. The abrasive steel balls made of 100Cr6 material and being Ø6 mm in diameter were utilized. The spherical balls were replaced for each test. The chemical composition and morphology of the wear surfaces were examined through SEM-EDS analyses. The wear trace thicknesses were measured using an optical microscope.

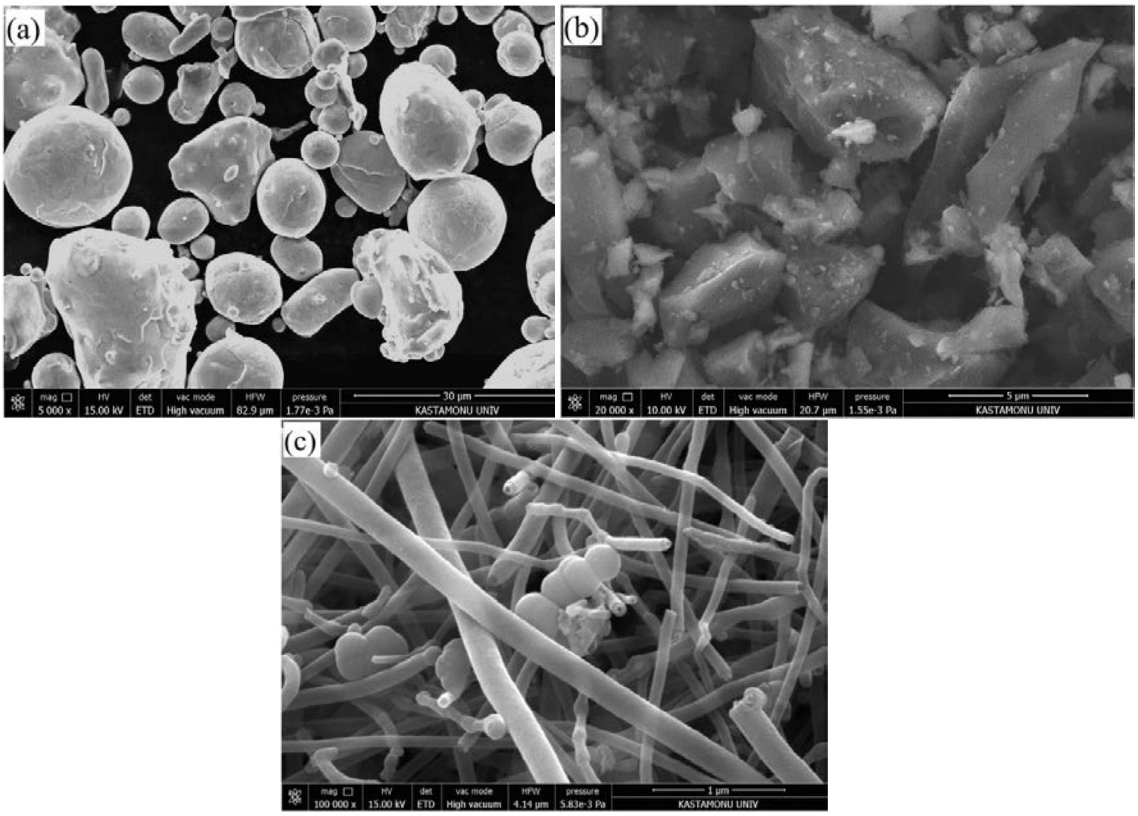

Fig. 1. SEM images of the powders: a) Ni, b) B_4C and c) CNF.

3. Results and Discussion

Fig. 2 shows the SEM images of Ni-B_4C/CNF composites produced by powder metallurgy (PM). Unavoidable pores in PM samples can also be observed in these samples. The unreinforced sample exhibited more pores than the other samples (Fig. 2a). This can be explained by the hard particles on the sanding paper pricking into the Ni matrix and then rupturing from the surface during the sanding of the pure Ni matrix. The pores in pure Ni were superficial. This is because the density results in the following sections indicated that the pure Ni sample was denser and had less porosity. The figure illustrates that there was a relatively visual reduction in pores as the CNF reinforcement increased (Fig. 2b-e). In the Ni matrix, B_4C particles were not seen very often. This can be explained as the formation of the boride phase between B and Ni in the decomposed B_4C. In small magnification rates it makes it harder to discern CNF in the microstructure. The detailed image in Fig. 2f shows that the CNFs were positioned at the contact points of nickel powders in high magnifications.

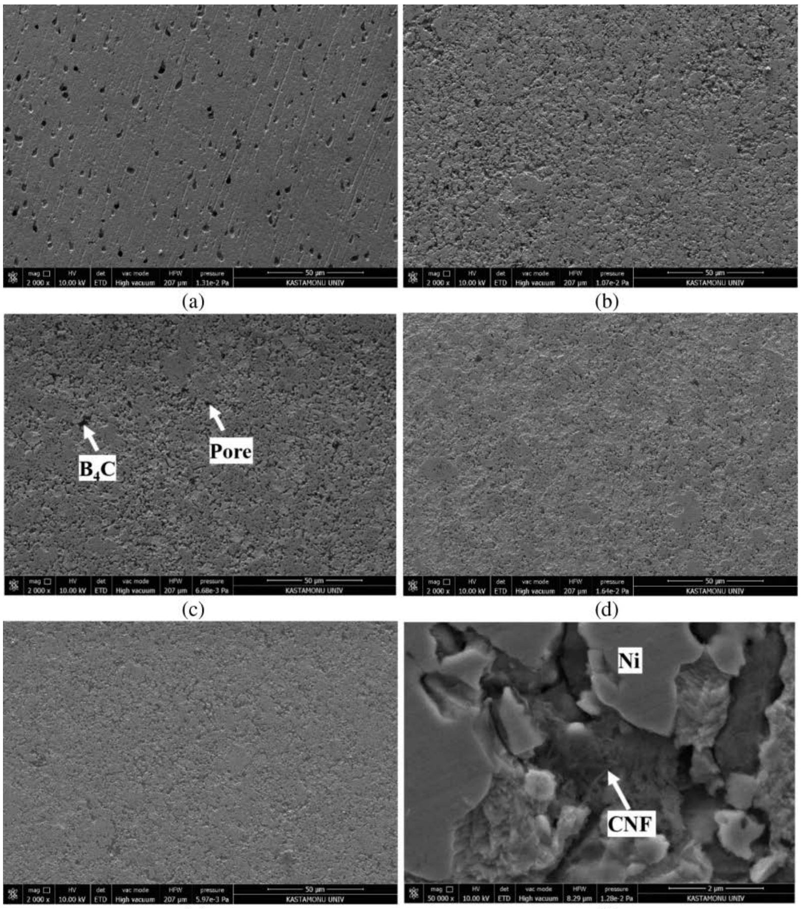

Fig. 2. SEM images of the samples: (a) 1, (b) 2, (c) 3, (d) 4, (e) 5 and (f) detail of sample No. 5.

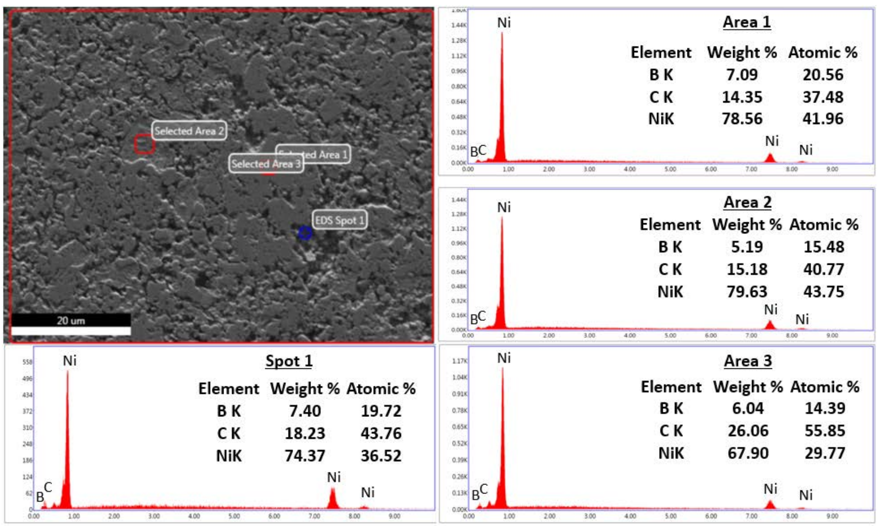

Fig. 3. The EDS analysis of sample No. 5.

Fig. 3 shows the EDS analysis of sample No. 5 (Ni-10B_4C-2CNF). The EDS results obtained from different zones and spots were close to each other. This may indicate a relatively homogeneous composition of each side of the sample. Given the EDS analysis of the entire surface, the sample surface was composed of 6.04 wt.% B, 26.06 wt.% C and 67.90 wt.% Ni. No oxides or impurities were found on the sample surface.

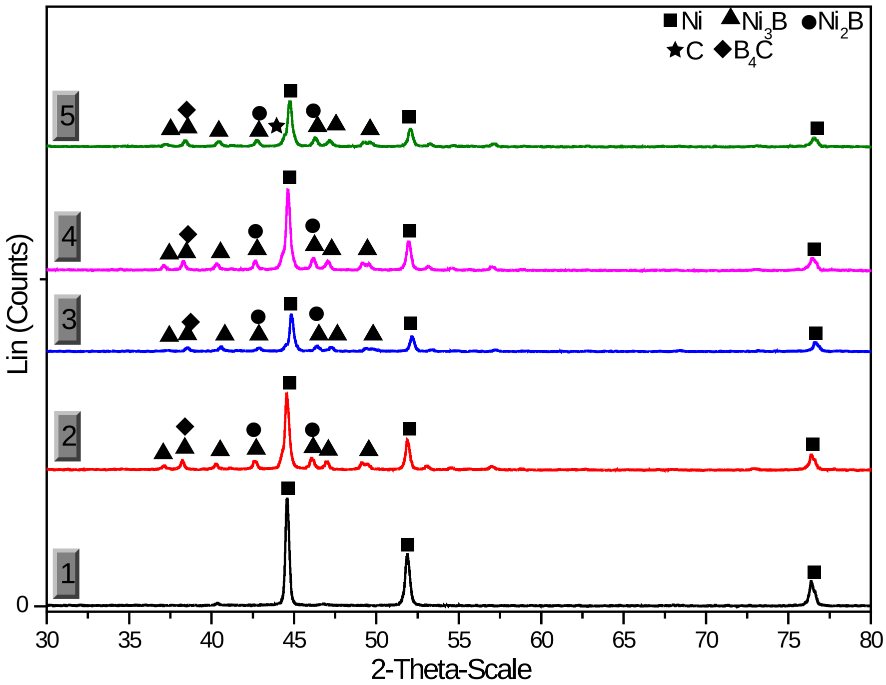

Fig. 4. XRD graph of the samples.

Fig. 4 shows the XRD analysis of Ni-B_4C/CNF composites produced by PM. The unreinforced matrix sample was composed of the Ni phase. The 2-theta values of the Ni phase are 44.582°, 51.902° and 76.377°. In addition to the Ni phase, Ni_2B, Ni_3B, B_4C, and C phases were identified in the microstructure when B_4C and CNF were reinforced. The Ni_2B phase was found at the 2-theta angles of 42.687° and 46.048°. The Ni_3B phase was identified at the 2-theta angles of 37.235°, 38.393°, 40.502°, 42.741°, 46.296°, 47.132° and 49.287°. The phases Ni_2B and Ni_3B were formed by the decomposition of B_4C and the reaction of B with Ni. In the study by Sandy et al. [12] on Ni-B_4C, they identified the phases Ni_2B and Ni_3B. In addition, Akkaş and Islak [5] reported the presence of Ni_2B and Ni_3B phases in the microstructure of NiB-TiC composites.

Fig. 5 shows the sample densities measured based on the Archimedes' principle as well as the relative densities calculated by proportioning the measured densities to theoretical densities. The sample densities ranged from 8.151 to 7.152. The relative densities, on the other hand, varied between 92 % and 88 %. The sintered density, as well as the relative density, both significantly reduced by adding B_4C into Ni (No. 2). The addition of CNF (samples No. 3, 4, 5) into the Ni-B_4C sample group resulted in, albeit slightly, an increase in sample densities and relative densities. In their study, Kwon et al. [13] discovered that in Al-CNF composites, addition of CNF reduced densities but increased them slightly via the extrusion method. CNFs had the ability to fill pores, in the current study.

The graph in Fig. 6 shows the hardness values of the samples. The graph indicates that adding B_4C and CNF to the Ni matrix significantly increased the hardness. The microhardness values of the sample groups (pure Ni, Ni-10B_4C, Ni-10B_4C-1CNF, Ni-10B_4C-1.5CNF and Ni-10B_4C-2CNF) were approximately 95 HV_1, 112 HV_1, 118 HV_1, 126 HV_1 and

137 HV_1, respectively. Ni-10B_4C-2CNF sample was approximately 44 % harder than unreinforced pure Ni sample. Here, it is clear that the Ni_2B and Ni_3B forming in the microstructure as well as externally added B_4C and CNF reinforcements increased hardness. The formed and externally added phase and particles inhibited the mobility of the dislocations, which result in an increase in hardness [14-16].

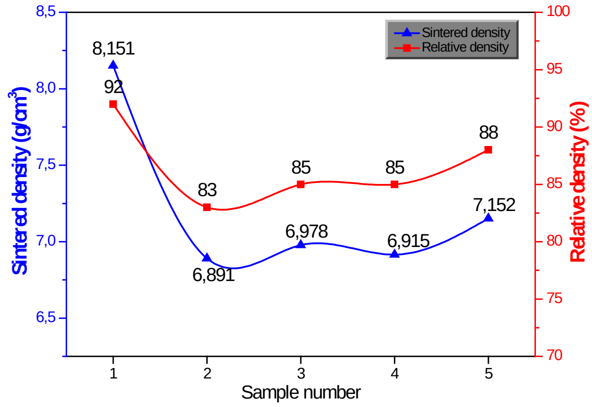

Fig. 5. Density graph of the samples.

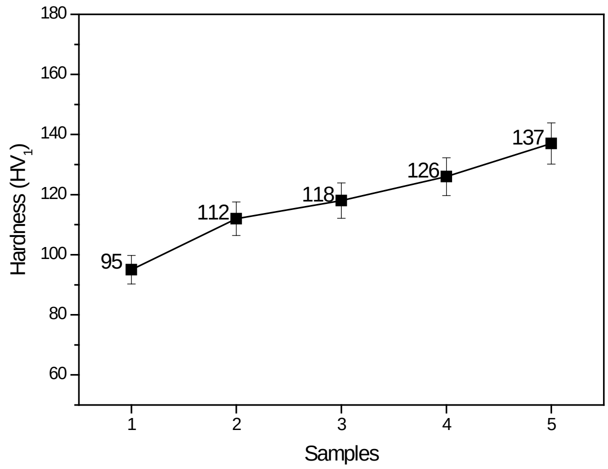

Fig. 6. Hardness graph of the samples.

Fig. 7 shows a graph of the friction coefficient- dislocation distance from the pin-on-disc wear test to determine the wear properties of the samples. The friction coefficient of the unreinforced sample No. 1 (Ni) was measured as 0.536. The friction coefficient for sample No. 2 formed by the addition of boride carbide to the nickel is 0.528, whereas the friction coefficients of the samples (No. 3, 4, and 5) obtained by adding CNF rates of 1, 1.5 and 2 wt% to the Ni-B_4C pair were measured as 0.566, 0.553, and 0.433, respectively. Here, after a CNF rate of 1.5 %, the friction coefficient appeared to have reduced significantly. This can be explained by the fact that the CNF rate should be above a certain limit to create a uniform tribofilm on the friction interface between the counter ball and the sample. The study by Lei et al. [17] on nickel-graphene composites reported a significant decrease in the friction coefficient after 0.99 % graphene. The lowest friction coefficient was achieved when 2 % CNF was added. This was based on the lubricating properties of carbon-based reinforcements, according to Scharf et al. [18]. The wear rate is a quantity that can be assessed for wear losses of samples. The wear rate is calculated based on the values, such as lost volume, applied load and wear distance [19-21]. The wear volume was calculated by taking into account the wear trace widths. Fig. 8 shows the wear track widths measured by using an optical microscope. For samples No. 1, 2, 3, 4 and 5, the wear track widths were, respectively, 1005 µm, 500 µm, 541 µm, 495 µm and 483 µm.

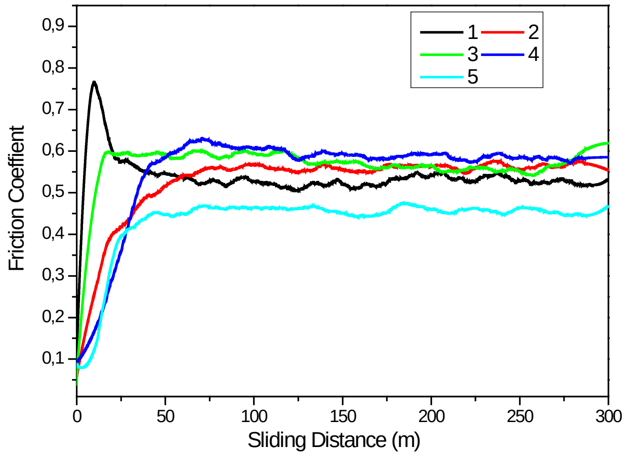

Fig. 7. Friction coefficient-distance graph of the samples.

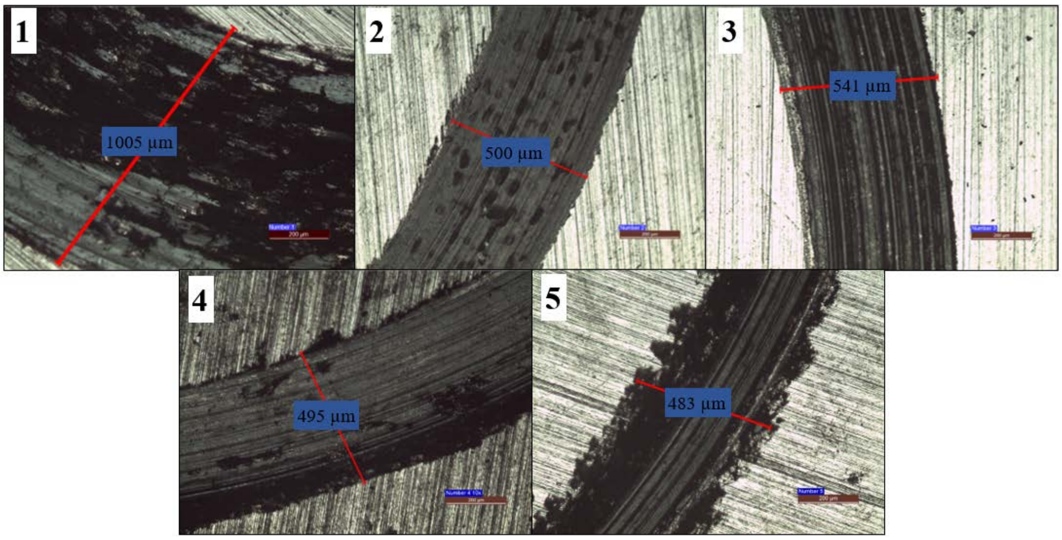

Fig. 8. Optic images of wear track widths.

Fig. 9 provides the graph of the wear rates of the samples. The wear rate of the reinforced samples was significantly lower than that of the unreinforced sample. This indicates that the wear resistance of the samples increased in B_4C and CNF reinforcements. The wear rate of the unreinforced sample was $2.623x10^{-4}$ mm^3 $(N.m)^{-1}$ but the wear rate was $0.322x10^{-4}$ mm^3. $(N.m)^{-1}$ with addition of 10 % B_4C. There was about an eight-fold reduction in the wear rate. When CNF of 1 %, 1.5 % and 2 % was added into the Ni-10B_4C composite, the wear rates were calculated as $0.373x10^{-4}$ mm^3. $(N.m)^{-1}$, $0.292x10^{-4}$ mm^3. $(N.m)^{-1}$ and $0.244x10^{-4}$ mm^3. $(N.m)^{-1}$, respectively. Here, the failure of CNFs to distribute homogeneously in the microstructure can be explained as the cause of the increase, albeit slightly, in the wear rate in addition of the 1 % CNF. When the unreinforced Ni and Ni-10B_4C-2CNF samples were compared, the wear rate was found to reduce by about 10.75-fold. Fig. 10 shows the morphologies of the wear surface of the unreinforced Ni-10B_4C-2CNF samples as well as the EDS analysis of the surface. In both samples, wear grooves and plastic deformation zones were observed. The grooves were wider and deeper in unreinforced pure Ni samples, while plastic deformation was more severe. In the Ni-10B_4C-2CNF sample, the grooves were superficial and the plastic deformation effect was less. Because hard phases and particles diminish the plastic deformation effect [22]. These indicators belong to the abrasive wear mechanism. The image in Fig. 10b also draws attention to the formation of cracks. This can be explained by the cracking of the sample that was hardened by boride and CNF due to the loading effect of the abrasive ball. The EDS analyses of the wear surfaces draw attention to the presence of high oxygen rate. This presence of oxide forms an oxide film and acts as a tribolayer [23-25].

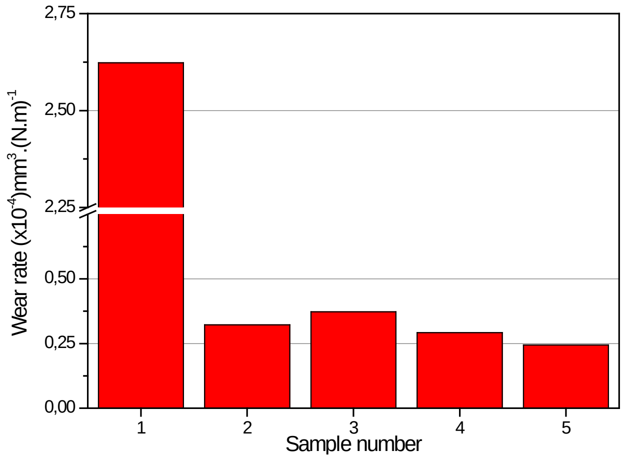

Fig. 9. Graph of wear rate of the samples.

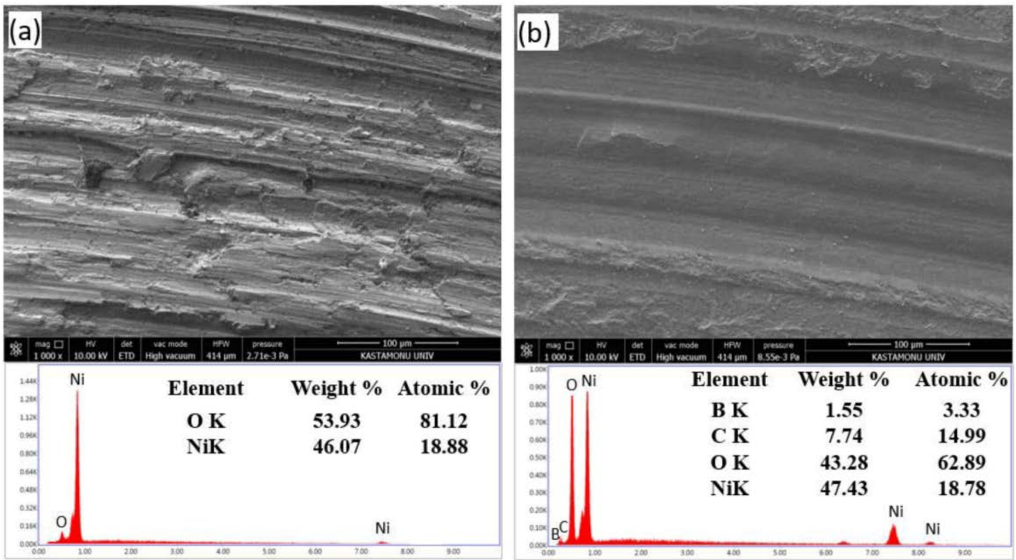

Fig. 10. SEM images of wear surfaces: No. a) 1 and b) 5.

4. Conclusion

The following results were obtained from the study on the wear and microstructure properties of Ni-B_4C/CNF composites produced with PM.

- CNFs are relatively homogeneously dispersed within the matrix. Since B_4C dissolves during production and forms an intermetallic phase (Ni_2B and Ni_3B) with Ni, a very small amount was detected in the matrix.
- While the densities decreased with the addition of B_4C to the Ni matrix, there was a slight increase in the densities with the addition of CNF. Ni_2B and Ni_3B formed in the microstructure and B_4C and CNF reinforcements added externally caused an increase in hardness.
- With the addition of B_4C and CNF to Ni, there was a general decrease in friction coefficients and wear rates. This is due to the formation of intermetallic phases in the body and the tribolayer effect of CNF and ixite layer.

5. References

1. X. Zhang, J. Ma, J. Yang, Q. Bi, W. Liu, Dry-sliding tribological behavior of Fe–28Al–5Cr/TiC composites, Wear 271 (2011) 881-888.
2. X. Zhang, J. Ma, L. Fu, S. Zhu, F. Li, J. Yang, W. Liu, High temperature wear resistance of Fe–28Al–5Cr alloy and its composites reinforced by TiC, Tribol. Int. 61 (2013) 48-55.
3. Z. Wu, L. Liu, B. Shen, Y. Wu, Y. Deng, C. Zhong, W. Hu, Mechanical behavior of α-Al_2O_3-coated SiC particle reinforced nickel matrix composites, J. Alloys Compd. 570 (2013) 81-85.
4. S. Islak, M. Ulutan, S. Buytoz, Microstructure and Wear Properties of Hot-Pressed NiCrBSi/TiC Composite Materials, Russ. J. Non-Ferr. Met. 61 (2020) 571-582.
5. M. Akkaş, S. Islak, Microstructure, wear and corrosion properties of NiB-TiC composite materials produced by powder metallurgy method, Sci. Sint. 51 (2019) 327-338.
6. S. Buytoz, M. Ulutan, S. Islak, B. Kurt, O.N. Çelik, Microstructural and wear characteristics of high velocity oxygen fuel (HVOF) sprayed NiCrBSi–SiC composite coating on SAE 1030 steel, Arab. J. Sci. Eng. 38 (2013) 1481-1491.
7. J. Jiang, X. He, J. Du, X. Pang, H. Yang, Z. Wei, In-situ fabrication of graphene-nickel matrix composites, Mater. Lett. 220 (2018) 178-181.
8. J. Nguyen, T.B. Holland, H. Wen, M. Fraga, A. Mukherjee, E. Lavernia, Mechanical behavior of ultrafine-grained Ni–carbon nanotube composite, J. Mater. Sci. 49 (2014) 2070-2077.
9. ASTM B962-17, Standard test methods for density of compacted or sintered powder metallurgy (PM) products using Archimedes' principle, ASTM International, 2017.
10. ASTM E92-17, Standard test methods for Vickers hardness and Knoop hardness of metallic materials. West Conshohocken (PA): ASTM International, 2017.
11. ASTM G99-17: Standard Test Method for Wear Testing with a Pin-on-Disk Apparatus, ASTM International, 2017.
12. K.A. Sandy, H. Henein, K.M. Jaansalu, On the Contact of Liquid Nickel with Tungsten Carbide or Boron Carbide, Can. Metall. Q. 48 (2009) 133-143.
13. H. Kwon, H. Kurita, M. Leparoux, A. Kawasaki, Carbon nanofiber reinforced aluminum matrix composite fabricated by combined process of spark plasma sintering and hot extrusion, J. Nanosci. Nanotechnol. 11 (2011) 4119-4126.
14. S. Islak, Ö. Küçük, Ö. Eski, C. Özorak, M. Akkaş, The Effect of CNT Content and Sintering Temperature on Some Properties of CNT-reinforced MgAl Composites, Sci. Sint. 49 (2017) 347-357.
15. S. Islak, Mechanical and corrosion properties of AlCu matrix hybrid composite materials, Sci. Sint. 51 (2019) 81-92.

16. M. Akkaş, S. F. R. A. Al, Effect of hot pressing and reinforcement of TiC and WC on the mechanical properties and microstructure of AlCuFeCrNi HEAs alloy, Sci. Sint. 53 (2021) 19-35.
17. Y. Lei, J. Jiang, T. Bi, J. Du, X. Pang, Tribological behavior of in situ fabricated graphene–nickel matrix composites, RSC Adv. 8 (2018) 22113-22121.
18. T.W. Scharf, A. Neira, J.Y. Hwang, J. Tiley, R. Banerjee, Self-lubricating carbon nanotube reinforced nickel matrix composites, J. Appl. Phys. 106 (2009) 013508.
19. F. Zhou, Y. Wang, F. Liu, Y. Meng, Z. Dai, Friction and wear properties of duplex MAO/CrN coatings sliding against Si_3N_4 ceramic balls in air, water and oil, Wear 267 (2009) 1581-1588.
20. S. Islak, Ö. Eski, V. Koç, C. Özorak, Wear properties and synthesis of CrFeNiMoTi high entropy alloy coatings produced by TIG process, Indian J. Eng. Mater. Sci. 27 (2020) 659-664.
21. S. Aksöz, S. Kaner, Y. Kaplan, Tribological and aging behavior of hybrid Al 7075 composite reinforced with B_4C, SiC, and TiB_2, Sci. Sint. 53 (2021) 311-321.
22. T. Borkar, S. Harimkar, Microstructure and wear behaviour of pulse electrodeposited Ni–CNT composite coatings, Surf. Eng. 27 (2011) 524-530.
23. A.R. Riahi, A.T. Alpas, The role of tribo-layers on the sliding wear behavior of graphitic aluminum matrix composites, Wear 251 (2001) 1396-1407.
24. C.H. Hager Jr, J. Hu, C. Muratore, A.A. Voevodin, R. Grandhi, The mechanisms of gross slip fretting wear on nickel oxide/Ti6Al4V mated surfaces, Wear 268 (2010) 1195-1204.
25. Y. Kaplan, S. Aksöz, H. Ada, E. İnce, S. Özsoy, The effect of aging processes on tribo-metallurgy properties of al based ternary alloys product by P/M technique, Sci. Sint. 52 (2020) 445-456.

Сажетак: *Циљ овог рада је да се испитају микроструктура и хабање бор карбида (B_4C) у матрици никла (Ni) и композита на бази карбонских (CNF) нановлакана. Микроструктура и фазни састав композита добијених металургијом праха (PM) су одређене уз помоћ SEM-EDS и XRD анализа. Тврдоћа композита је одређена методом по Викерсу, а хабање методом игла-на-диску. SEM микрографије указују на хомогену расподелу B_4C, док се CNF акумулира на неким деловима, или у малој количини. Додатак B_4C и CNF у матрицу то нагомилавање додатно појачавају. Тврдоћа је знатно нижа са додатком CNF. Према резултатима хабања, ојачање Ni матрице редукује стопу хабања и коефицијент фрикције.*
Кључне речи: *никл, карбонска нановлакна, бор карбид, хабање, композити.*